were substituted with Arg, could be used to ubiquitinate L3MBTL1 (Figures S5A and S5B). When His-L3MBTL1, which was purified from U2OS cells under denaturing condition, was incubated in the presence of recombinant UBCH5c in vitro, His-L3MBTL1 was multiply ubiquitinated by K0 ubiquitin and Octa-dimethyl-ubiquitin that is unable to form ubiquitin chains via linkages with other ubiquitin molecules (Figures S5C and S5D). These data suggest that L3MBTL1 is atypically and likely multiply ubiquitinated. When OTUB2 was coexpressed with His-L3MBTL1, HA-RNF8, and Myc-ubiquitin in U2OS cells, L3MBTL1 ubiquitination was significantly suppressed, and this suppression was dependent on the DUB activity of OTUB2 (Figure 5C). In addition, DSB-induced L3MBTL1 ubiquitination (Acs et al., 2011) was also antagonized by OTUB2 in a DUB activity-dependent manner (Figures 5D, S5E, and S5F).

Finally, we investigated whether OTUB2 could deubiquitinate L3MBTL1 in vitro. When in vivo ubiquitinated L3MBTL1 was incubated with recombinant OTUB2 proteins, recombinant OTUB2 decreased the amount of ubiquitinated L3MBTL1 and generated ubiquitin monomers (Figure 5E). In contrast, $OTUB2^{C51S}$ and OTUB1 did not induce these changes. When in vitro ubiquitinated L3MBTL1, which was detected as a smear by L3MBTL1 immunoblotting, was incubated with recombinant His-OTUB2 protein, L3MBTL1 was deubiquitinated and detected as a sharp band by immunoblotting (Figure S5G). These data indicate that OTUB2 removes ubiquitins that directly bind to L3MBTL1. Thus, OTUB2 deubiquitinates L3MBTL1 in vivo and in vitro. Because ubiquitination of L3MBTL1 is a prerequisite for L3MBTL1 removal from damaged chromatin (Acs et al., 2011), we conclude that OTUB2 deubiquitinates L3MBTL1 and suppresses the accelerated removal of L3MBTL1 from damaged chromatin.

OTUB2 Suppresses Lys 63-Linked Ubiquitin Chain Synthesis but Not Histone H2A Ubiquitination

The recruitment of 53BP1 to DSBs also requires the RNF168-dependent multiubiquitination of Lys 13-15 on histone H2A (Fradet-Turcotte et al., 2013; Mattiroli et al., 2012). Therefore, we asked whether OTUB2 also negatively regulates histone H2A ubiquitination. Although the accumulation of RNF168 at DSBs depends on the E3 ligase activity of RNF8, overexpression of RNF168 can transmit a DDR signal in the absence of RNF8 (Stewart et al., 2009). Utilizing this feature, we performed an in vivo histone ubiquitination assay in 293T cells and U2OS cells that overexpressed OTUB2 and had suppressed RNF8-dependent ubiquitination. In this assay, cells were transfected with RNF168- and Myc-ubiquitin-expressing plasmids, and then histones were extracted from the cells through acid extraction. The extracted histones were subjected to SDS-PAGE and immunoblotting, in which the ubiquitinated histones were detected using the anti-Myc antibody (Nakada et al., 2010). Whereas the exogenous expression of OTUB1 completely abrogated RNF168-dependent histone ubiquitination, the exogenous expression of OTUB2 did not affect the histone ubiquitination level (Figures 5F and S5H).

Next, we examined whether OTUB2 is able to antagonize synthesis of the Lys 63-linked ubiquitin chain. The in vitro synthesis of Lys 63-linked polyubiquitin chains mediated by the UBC13/UEV1a heterodimer was inhibited by recombinant OTUB2 protein in a DUB activity-dependent manner (Figure 5G). Furthermore, recombinant OTUB2 efficiently cleaved Lys 63-linked tetra-ubiquitin in vitro (Figure 5H). These data, combined with the observation that NCS-induced formation of RAP80 foci was inhibited by OTUB2 overexpression (Figures 2C and 2D) and accelerated by OTUB2 depletion (Figures 3A and 3B), indicate that OTUB2 negatively regulates DNA damage-dependent Lys 63-linked ubiquitin chain synthesis.

OTUB2 Depletion Promotes Early-Phase DSB Repair but Suppresses HR

OTUB2-depleted cells exhibited faster dissolution of conjugated ubiquitin foci post-NCS treatment (Figure 3G), suggesting that DSB repair may be quicker in OTUB2-depleted cells than in control cells. To investigate whether DSB repair efficiency in an early phase of the DDR is affected by OTUB2 depletion, we measured DSB repair kinetics with the neutral comet assay. In this assay, XRCC4-depleted cells, in which NHEJ is impaired (Goodarzi and Jeggo, 2013), showed slower DSB repair post-NCS treatment (Figures 6A and S6A). As expected, OTUB2-depleted cells showed better DSB repair efficiency 2 hr post-NCS treatment. This faster DSB repair was reversed by pharmacological inhibition of DNA-PKcs, which is required for NHEJ (Figure 6B). U2OS cells simultaneously transfected with siRNAs for 53BP1, RAP80, and OTUB2 showed more inefficient DSB repair 2 hr post-NCS treatment than U2OS cells simultaneously transfected with OTUB2-specific siRNA and control siRNA (Figures 6C and S6B), suggesting that faster DSB repair in OTUB2-depleted cell depends on RAP80 and/or 53BP1. Consistent with the comet assay data, OTUB2 depletion accelerated the dissociation kinetics of γH2AX foci (Figure 6D), which is generally considered to reflect DSB repair (Beucher et al., 2009).

Although early-phase DSB repair is promoted in OTUB2-depleted cells, accumulating evidence suggests that the enhanced recruitment of RAP80 and 53BP1 should suppress HR (Chapman et al., 2013; Coleman and Greenberg, 2011; Di Virgilio et al., 2013; Escribano-Díaz et al., 2013; Hu et al., 2011; Zimmermann et al., 2013). To investigate whether HR is promoted or suppressed in OTUB2-depleted cells, we analyzed

Figure 3. OTUB2 Silencing Accelerates RNF8-Dependent Ubiquitination and Enhances the Recruitment of RAP80 to DSBs in an Early Phase of the DDR

(A–H) In (A), (C), (E), and (H), U2OS cells transfected with the indicated siRNAs were treated with 5 ng/mL NCS and processed for the indicated protein immunofluorescence staining at the indicated time points after NCS treatment. Representative images of the immunofluorescence staining are shown. The nuclei are outlined. Scale bar, 25 μm. In (B), (D), (F), and (G), quantification of cells with the indicated protein foci is shown. The percentage of cells containing > 10 or >20 foci was determined by counting 300 cells from each sample. Data are presented as the mean ± SD of three independent experiments. $^*p < 0.05$, n.s.; not significant: Kruskal-Wallis test; p values are adjusted for multiple comparisons by the Steel method. See also Figure S3.

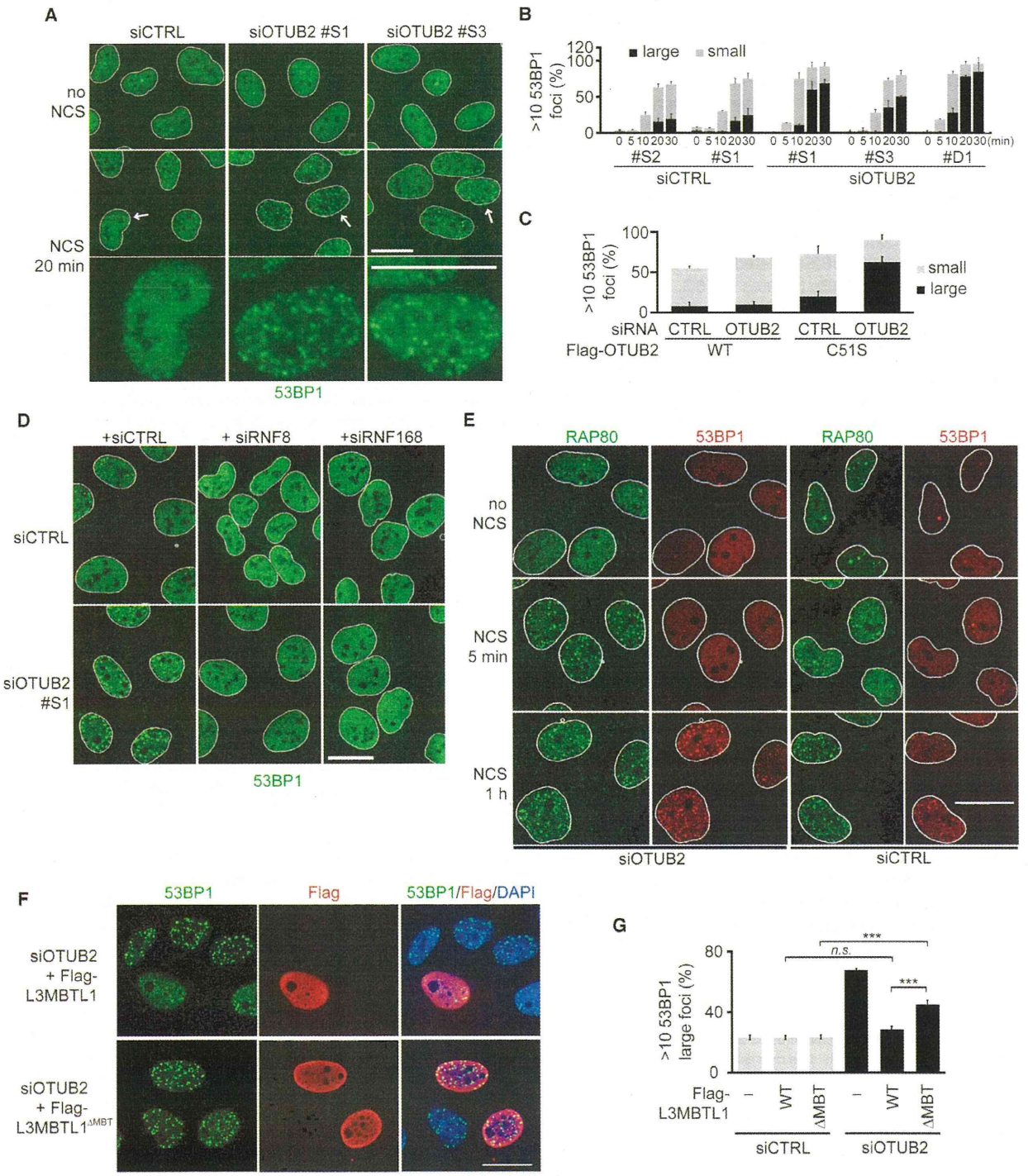

Figure 4. OTUB2 Silencing Accelerates the Recruitment of 53BP1 to DSBs

(A) U2OS cells transfected with the indicated siRNAs were treated with 5 ng/mL NCS and processed for 53BP1 immunofluorescence staining at the indicated time points after NCS treatment. Representative images of the immunofluorescence staining are shown. The nuclei are outlined. The cells indicated by arrows are magnified in the bottom row. The bottom image in the left column represents an image of cells with small 53BP1 foci. The bottom images in the middle and right columns present images of cells with large foci. Scale bar, 25 μm.

(legend continued on next page)

the efficiency of HR using a direct repeat-green fluorescent protein (DR-GFP) reporter integrated into HeLa cells. In this assay, when a single DSB is induced by the exogenously expressed I-SceI endonuclease and repaired by HR, cells express GFP protein (Pierce et al., 1999). The depletion of OTUB2 led to a reduction in GFP-positive DR-HeLa cells after exogenous expression of I-SceI (Figure 6E). The smaller population of S and G2 phase cells leads to an apparent reduction in HR efficiency in the DR-GFP assay; in contrast, OTUB2-depleted cells showed a larger population of S and G2 phase cells (Figure S6E). We conclude that OTUB2 is required for efficient HR. Furthermore, OTUB2-depleted cells exhibited inefficient RAD51 assembly at DSBs (Figures 6F, 6G, and S6C), which is a critical step for HR. Although many siRNAs have off-target effects on RAD51 stability (Adamson et al., 2012), cells transfected with OTUB2 siRNA did not show a decrease in the level of RAD51 or other HR-related proteins (Figure S6F). Additionally, RPA accumulation at DSBs and phosphorylation of RPA were also suppressed in OTUB2-depleted cells (Figures 6H, 6I, S6D, and S6G), strongly suggesting that DNA end resection was suppressed in OTUB2-depleted cells. Because the cell-cycle distribution was comparable among cells transfected with the control or OTUB2-specific siRNAs (Figures S6H and S6I), it is unlikely that the percentage of RAD51- or RPA foci-positive cells was affected by differences in cell-cycle distribution. Because the depletion of 53BP1 and/or RAP80 from OTUB2-depleted cells rescued the defects in RAD51 and RPA foci formation (Figures 6J, 6K, and S6J–S6M), we conclude that accelerated ubiquitination suppresses DNA end resection in a 53BP1- and RAP80-dependent manner in the absence of OTUB2.

Lastly, we examined the impact of OTUB2 depletion on cellular resistance to DNA damaging agents. OTUB2-depleted cells did not show hypersensitivity to NCS (Figure 7A). In contrast, OTUB2-depleted cells showed hypersensitivity to the topoisomerase I inhibitor camptothecin (Figure 7B). Camptothecin stabilizes single-stranded DNA breaks within the topoisomerase I cleavage complex. Because the camptothecin-induced breaks were converted to DSBs through replication, which were subsequently repaired by HR (Pommier, 2006), we conclude that the camptothecin sensitivity of OTUB2-depleted cells reflects the impact of OTUB2 on HR.

DISCUSSION

Accelerated Ubiquitination Promotes Non-HR DSB Repair and Suppresses HR

The choice of an appropriate repair pathway is required for maintaining genomic integrity (Chapman et al., 2012). Although the detailed molecular mechanism of repair pathway choice remains unclear, competition between DNA-end protection and DNA-end resection seems to determine the choice (Symington and Gautier, 2011). 53BP1 and RAP80 participate in this process. RAP80 forms a protein complex with the HR-promoting factor BRCA1 (Kim et al., 2007; Sobhian et al., 2007; Wang et al., 2007). Nevertheless, depletion of RAP80 increases the efficiency of BRCA1-dependent DNA end resection and HR (Coleman and Greenberg, 2011; Hu et al., 2011), indicating that RAP80-BRCA1 interaction protects DNA ends rather than promoting resection. ATM-dependent phosphorylation of 53BP1 recruits RIF1 to DSBs. RIF1 accumulation suppresses the recruitment of the BRCA1-BARD1 complex to DSBs, inhibits DNA-end resection, and drives NHEJ (Chapman et al., 2013; Escribano-Díaz et al., 2013; Zimmermann et al., 2013). The function of RIF1 is prominent in cells in the G1 phase, during which proper HR does not occur. However, depletion of RIF1 or 53BP1 from BRCA1-depleted cells improves DNA damage-dependent RAD51 foci formation and resistance to a PARP inhibitor (Bouwman et al., 2010; Bunting et al., 2010; Escribano-Díaz et al., 2013), suggesting that the RIF1-53BP1 complex potentially protects DNA ends from resection not only in G1 but also in S and G2 phases.

In this study, we reveal that accelerated accumulation of 53BP1 and RAP80 induces faster DSB repair when RNF8-depedent ubiquitination is enhanced by OTUB2 depletion. Because DNA-end resection and HR are suppressed and the faster DSB repair depends on DNA-PKcs in OTUB2-depleted cells, we deduce that most of the accelerated DSB repair is performed by non-HR repair such as NHEJ (Goodarzi and Jeggo, 2013). The impact of OTUB2 depletion on the formation of RAP80 and 53BP1 foci is limited to an early phase of the DDR, suggesting that some DSBs, which are to be repaired by HR in the presence of OTUB2, are rapidly repaired by non-HR repair; therefore, the requirement for HR may be reduced in the absence of OTUB2. When cells are treated with NCS and two-ended DSBs are generated, most of the DSBs are repaired

(B) Quantification of cells with large or small 53BP1 foci shown in (A). The percentage of cells containing >10 53BP1 foci was determined by counting 300 cells from each sample. Data are presented as the mean ± SD of three independent experiments.
(C) Quantification of cells with large or small 53BP1 foci. siRNA-resistant Flag-OTUB2 or OTUB2^{C51S} mutant was introduced into U2OS cells transfected with siCTRL or siOTUB2 #S1. The cells were treated with 5 ng/mL NCS and processed for Flag and 53BP1 immunofluorescence staining 20 min after NCS treatment. The percentage of cells containing >10 53BP1 foci was determined by counting 100 cells with weak Flag-OTUB2 expression in each sample. Data are presented as the mean ± SD of three independent experiments.
(D) U2OS cells transfected with siOTUB2 #S1 and RNF8, RNF168, or control (CTRL) siRNA were subjected to 53BP1 immunofluorescence staining 20 min after NCS treatment. Representative images of the immunofluorescence staining are shown. The nuclei are outlined. Scale bar, 25 μm.
(E) U2OS cells transfected with siOTUB2 #S1 were treated with 5 ng/mL NCS and processed for RAP80 and 53BP1 immunofluorescence staining at the indicated time points after NCS treatment. Representative images of the immunofluorescence staining are shown. The nuclei are outlined. Scale bar, 25 μm.
(F) Flag-L3MBTL1 or L3MBTL1$^{\Delta MBT}$ mutant was introduced into U2OS cells transfected with siOTUB2 #S1. The cells were treated with 5 ng/mL NCS and processed for Flag and 53BP1 immunofluorescence staining 20 min after NCS treatment. The DNA was counterstained with DAPI. Representative images of the immunofluorescence staining are shown. Scale bar, 25 μm.
(G) Quantification of the cells with large 53BP1 foci shown in (F). The percentage of cells containing >10 large 53BP1 foci was determined by counting 100 cells with Flag-L3MBTL1 expression in each sample. Data are presented as the mean ± SD of three independent experiments. ***$p < 0.001$, n.s.; not significant: one-way analysis of variance; p values are adjusted for multiple comparisons by the Bonferroni method. See also Figure S4.

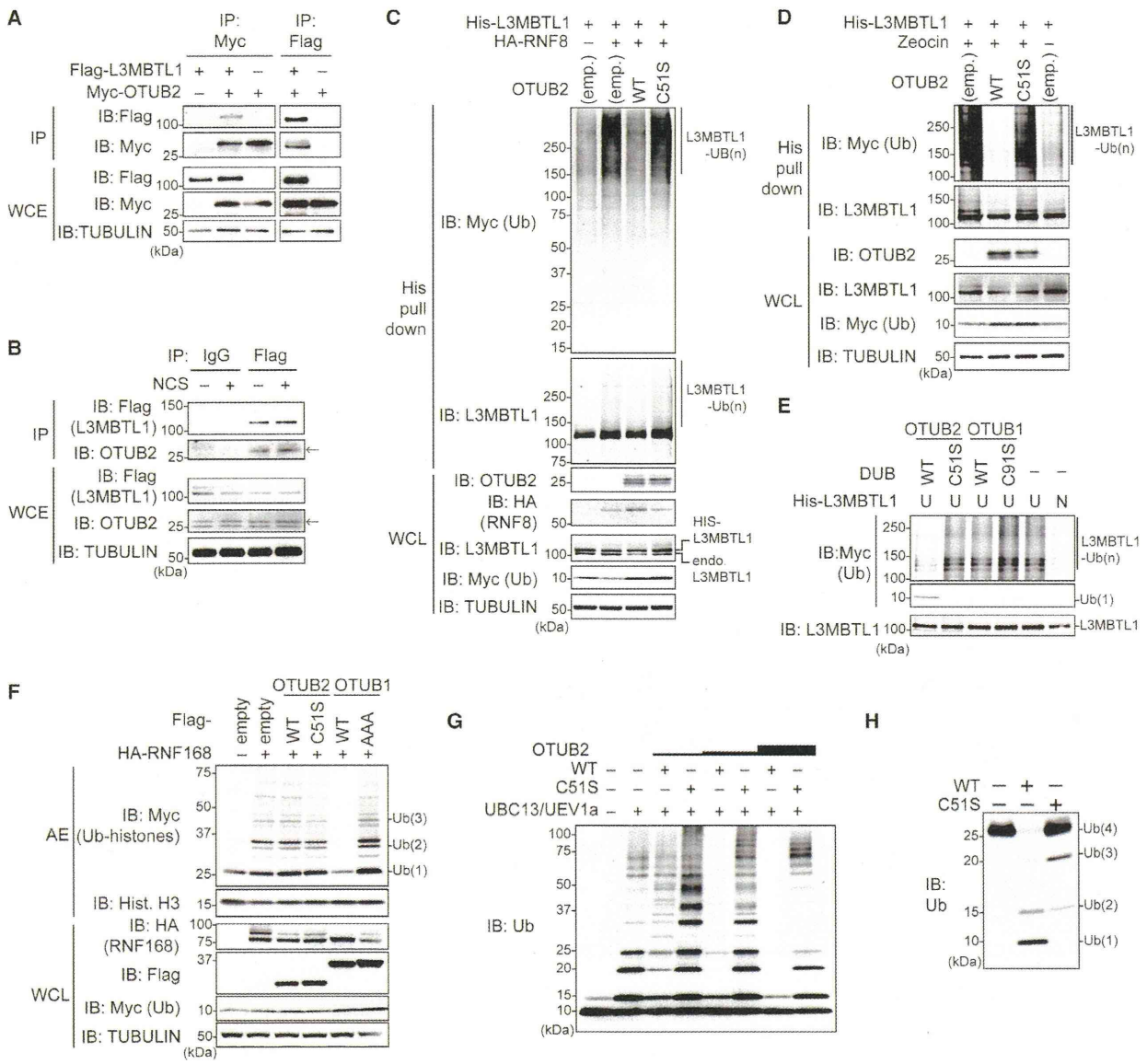

Figure 5. OTUB2 Suppresses L3MBTL1 Ubiquitination and Lys 63-Linked Ubiquitin Chain Synthesis

(A) U2OS cells cotransfected with Flag-L3MBTL1 and Myc-OTUB2 were subjected to Flag or Myc immunoprecipitation (IP) and subsequently analyzed by immunoblotting (IB). WCE, whole cell extract.

(B) U2OS cells stably expressing Flag-L3MBTL1 were treated with or without 500 ng/mL NCS, subjected to Flag immunoprecipitation, and subsequently analyzed by immunoblotting (IB) using OTUB2 antibodies. The arrow indicates the OTUB2-specific signal. WCE, whole cell extract.

(C) U2OS cells cotransfected with His-L3MBTL1, HA-RNF8, Myc-ubiquitin (Ub), and OTUB2 expression plasmids were subjected to His pull down and subsequently analyzed by immunoblotting (IB). WCL, whole cell lysate.

(D) U2OS cells cotransfected with His-L3MBTL1, Myc-ubiquitin (Ub), and OTUB2 expression plasmids were treated with 2 mM Zeocin for 30 min, subjected to His pull down, and subsequently analyzed by immunoblotting (IB). WCL, whole cell lysate.

(E) In vitro deubiquitination assays with in vivo ubiquitinated L3MBTL1 and recombinant OTUB2. The reaction mixtures were analyzed by immunoblotting (IB). U, L3MBTL1 ubiquitinated in the presence of RNF8, N, nonubiquitinated L3MBTL1.

(F) In vivo histone ubiquitination assay. Histones were isolated from 293T cells cotransfected with HA-RNF168, Myc-ubiquitin, and Flag-OTUB2 or OTUB1 expression plasmids by acid extraction (AE), and the acid-extracted proteins were analyzed by immunoblotting (IB) using the indicated antibodies. WCL, whole cell lysate.

(G) In vitro ubiquitination assays with combinations of UBE1, UBC13/UEV1a, and ubiquitin performed in the absence or presence of recombinant OTUB2 or OTUB2^{C51S}. The reaction mixtures were analyzed by immunoblotting (IB) using ubiquitin (Ub) antibody.

(H) In vitro deubiquitination assay. Lys 63-linked tetra-ubiquitin was incubated with recombinant OTUB2 or OTUB2^{C51S}. The reaction mixtures were analyzed by immunoblotting (IB) using ubiquitin (Ub) antibody.See also Figure S5.

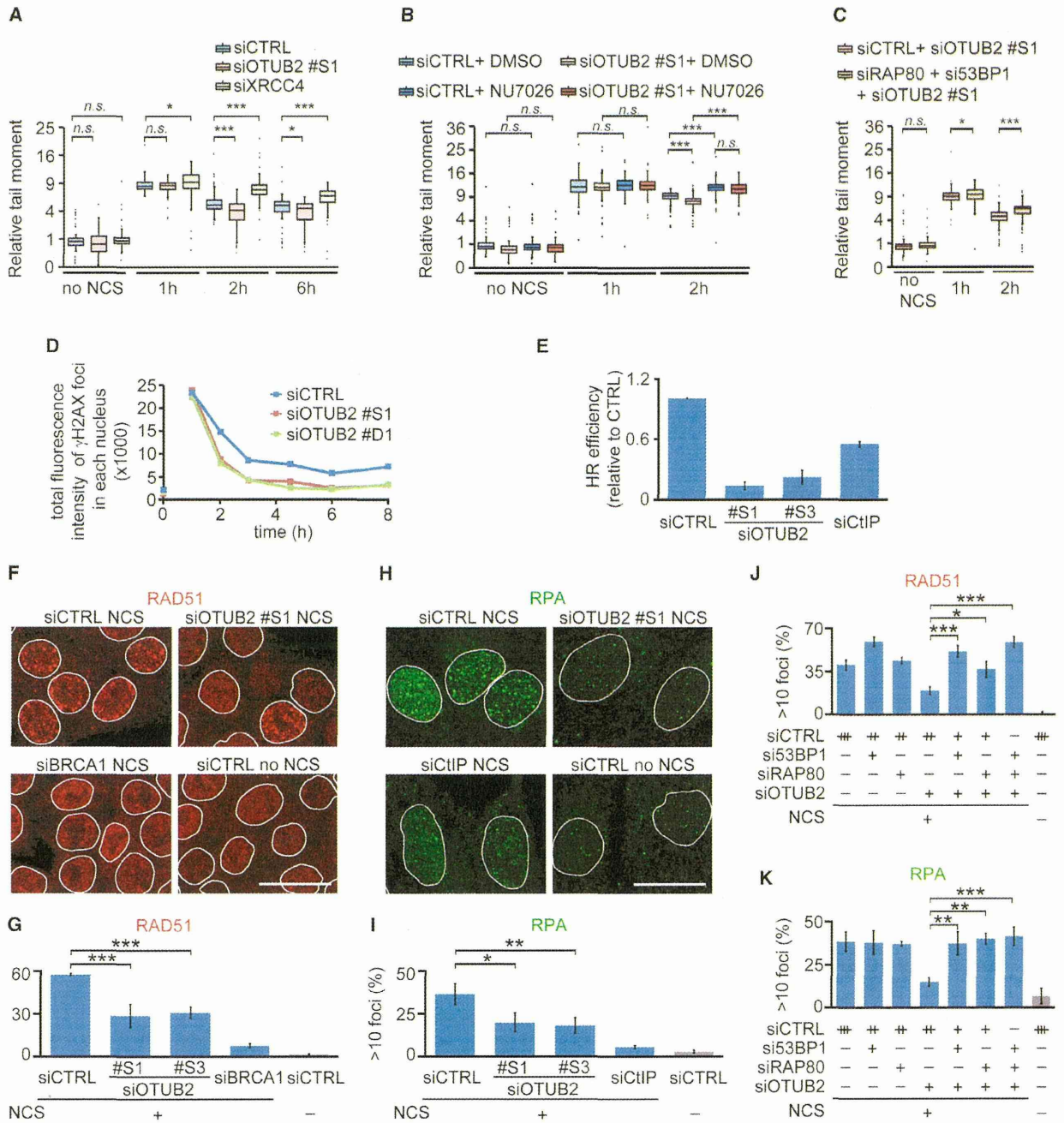

Figure 6. OTUB2 Silencing Promotes Early-Phase DSB Repair and Suppresses HR

(A–C) U2OS cells were treated with 500 ng/mL NCS for 30 min and collected at the indicated times after NCS treatment for neutral comet assays. Cell were treated with NU7026 (DNA-PKcs inhibitor) or DMSO 30 min prior to NCS treatment in (B). Quantification of the comet tail moments of the experiments is shown. Tail moments are normalized against the average comet tail moment of the mock-treated siCTRL-transfected cells and shown as a box and whisker plot. Outliers are indicated as dots. The ordinate is a square root scale. $^{*}p < 0.05$, $^{**}p < 0.01$, $^{***}p < 0.001$; n.s.; not significant: Kruskal-Wallis test; p values are adjusted for multiple comparisons by the Steel method.

(D) Quantification of γH2AX foci intensity. U2OS cells transfected with the indicated siRNAs were subjected to γH2AX immunofluorescence staining at the indicated time points after treatment with 5 ng/mL NCS. The total intensity of γH2AX foci in each nucleus was analyzed. Data are presented as the mean ± SEM. More than 300 cells in each sample were analyzed. All SEMs are less than 50.

(E) DR-HeLa cells transfected with the indicated siRNAs were subjected to a DR-GFP assay. Data are presented as the mean ± SD of three independent experiments.

(legend continued on next page)

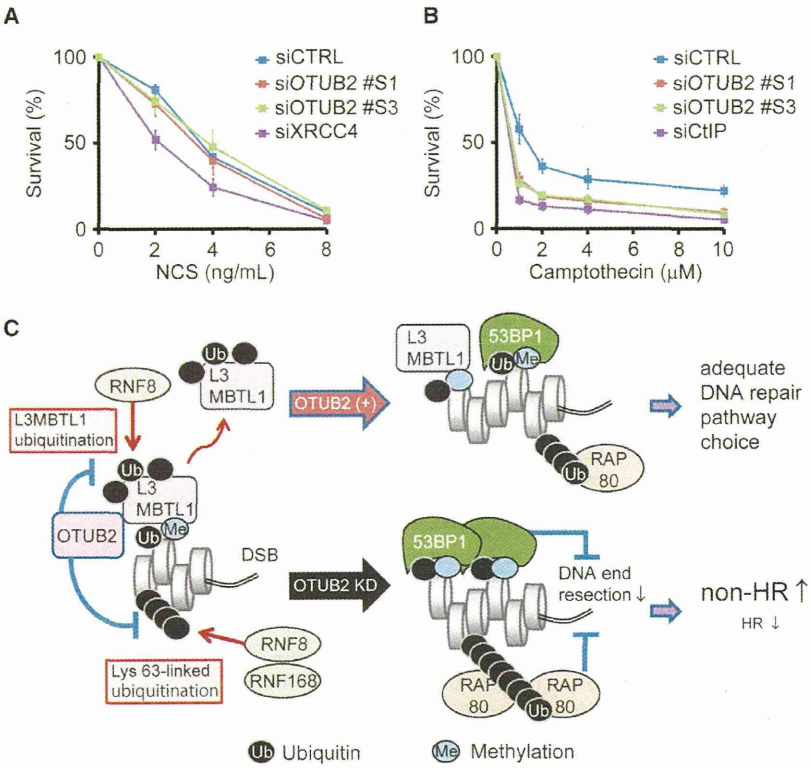

Figure 7. OTUB2-Depleted Cells Show Hypersensitivity to Camptothecin

(A and B) U2OS cells transfected with the indicated siRNAs were subjected to cell survival assays using NCS or camptothecin. Data are presented as the mean ± SD of three independent experiments.

(C) Model of OTUB2 action. Details are described in Figure S7.

by non-HR repair. Therefore, OTUB2-depleted cells are not sensitive to NCS. In contrast, camptothecin-induced single-strand DNA breaks are converted to DSBs through replication. Because inappropriate engagement of the NHEJ pathway following replication fork collapse leads to genome rearrangements and cell death (Saberi et al., 2007), OTUB2-depleted cells show sensitivity to camptothecin. Taking these findings together, we propose a model whereby OTUB2 inhibits excessive DSB-end protection and allows the initiation of HR by properly regulating the accumulation of RAP80 and 53BP1 at DSBs in an early phase of the DDR.

OTUB2 and OTUB1 Differentially Regulate the Ubiquitination-Dependent DDR

Because OTUB2 constitutively interacts with L3MBTL1, one of the physiological roles of OTUB2 may be to remove the ubiquitin that is unexpectedly conjugated to L3MBTL1 in the absence of DSBs. This feature enables OTUB2 to suppress convulsive RNF8-dependent L3MBTL1 ubiquitination immediately after the generation of DSBs. A slight increment in OTUB2 at sites of DSB, which can be detected only by micro-laser irradiation, probably elevates overall DUB activity of OTUB2 to respond the DSB-induced ubiquitination of L3MBTL1. However, the local concentration of OTUB2 at a DSB site should not be so high as to completely inhibit RNF8-mediated ubiquitination. OTUB2 only works as a mild suppressor of convulsive ubiquitination. We speculate that a similar mechanism exists for suppressing the DNA damage-dependent synthesis of the Lys 63-linked ubiquitin chain to which RAP80 binds. Further, conjugated ubiquitin foci are rapidly dissolved even in the absence of OTUB2, suggesting that other DUBs, such as BRCC36 (Shao et al., 2009) but not OTUB2, are responsible for the removal of ubiquitin after DNA repair.

While OTUB2 antagonizes DSB-induced ubiquitination through deubiquitination, a closely related otubain family member DUB, OTUB1, suppresses DSB-induced ubiquitination by inhibiting the E2-conjugating enzymes in a DUB activity-independent manner (Nakada et al., 2010). A recent study revealed that free ubiquitin binding to a second ubiquitin binding site in OTUB1 induces a conformational change in the N-terminal region of OTUB1, after which the protein can bind to ubiquitin-charged UBC13 more tightly, thereby inhibiting UBC13 activity (Wiener et al., 2012). This finding implies that a local increase in the concentration of free ubiquitin, which can be produced by deubiquitination at DSBs, terminates UBC13-dependent ubiquitination by activating the noncatalytic function of OTUB1 (Figure S7). If this interpretation is accurate, then OTUB1 should act in a later phase of the DDR, as opposed to an early phase. Indeed, conjugated ubiquitin foci persist until the recovery phase of the DDR in OTUB1-depleted cells. Thus, two closely related otubain family DUBs, OTUB1 and OTUB2, have separate roles in fine-tuning DSB-dependent ubiquitination.

(F–K) In (F), HCT116 cells transfected with the indicated siRNAs were treated with 20 ng/mL NCS and processed for RAD51 immunofluorescence staining 6 hr after NCS treatment. Representative images of the immunofluorescence are shown. The nuclei are outlined. Scale bar, 25 μm. In (G) and (J), quantification of the cells with RAD51 foci is shown. The percentage of cells containing >10 RAD51 foci was determined by counting 300 cells from each sample. Data are presented as the mean ± SD of three independent experiments. In (H), U2OS cells transfected with siOTUB2 #S1 and the indicated siRNAs were treated with 10 ng/mL NCS and processed for RPA immunofluorescence staining 4 hr after NCS treatment. Representative images of the immunofluorescence are shown. The nuclei are outlined. Scale bar, 25 μm. In (I) and (K), quantification of the cells with RPA foci is shown. The percentage of cells containing >10 RPA foci was determined by counting 300 cells from each sample. Data are presented as the mean ± SD of three independent experiments. $^{*}p < 0.05$, $^{**}p < 0.01$, $^{***}p < 0.001$: one-way analysis of variance; p values are adjusted for multiple comparisons by the Bonferroni method. See also Figure S6.

Collectively, our data establish that accelerated ubiquitination in an early phase of the DDR affects DNA repair pathway choice. OTUB2 opposes RNF8 through deubiquitination and fine-tunes the ubiquitination of L3MBTL1 and Lys 63-linked ubiquitin chain synthesis at DSBs to achieve an environment in which the appropriate DNA repair pathway can be chosen (Figure 7C).

EXPERIMENTAL PROCEDURES

siRNAs and shRNAs

We used the following siRNAs: siOTUB2 #S1: CAGAGUGCCUCGGACCACA (Hs01_00010701, Sigma-Aldrich), siOTUB2 #S3: CAUCCUUUAUGCAGCC GAU (Hs01_00010703, Sigma-Aldrich), siOTUB2 #D1: CCGUUUACCUGCU CUAUAA, siOTUB1: CCGACUACCUUGUGGUCUA, siRNF8: GGAGAUAG CCCAAGGAGAA, siRNF168: GGCGAAGAGCGAUGGAAGA, siCtIP: GCUA AAACAGGAACGAAUC, siXRCC4: AUAUGUUGGUGAACUGAGA, siBRCA1: GGAACCUGUCUCCACAAAG and siCTRL (#2) and siCTRL #1: MISSION siRNA Universal Negative Control 2 and 1 (SIC-002 and SIC-001, Sigma-Aldrich). The siGENOME SMARTpool siRNA Library Human Deubiquitinating Enzymes (G-004705, Lot 10117) and siGENOME Non-Targeting siRNA Pool were purchased from Thermo. L3MBTL1 (TRCN0000016867) and nontargeting shRNA constructs were obtained from Sigma-Aldrich.

Antibodies

We used the following antibodies: Flag (F3165, Sigma-Aldrich), DDDDK-tag (PM020, MBL), Myc (sc-40, Santa Cruz Biotechnology), conjugated ubiquitin (302-06751 [FK2], Nippon Biotest Laboratories), 53BP1 (NB100-305, Novus Biologicals; 612523 [19], BD Biosciences), RAP80 (NBP1-87156, Novus), RPA32 (NA18, Calbiochem) and RAD51 (70-001 lot 1, Bio Academia). All the antibodies used in this study are listed in Table S1.

Immunofluorescence Staining

Cells were usually fixed by incubation in 3% paraformaldehyde and 2% sucrose in PBS for 15 min at room temperature. The cells were permeabilized by incubation in 0.5% Triton X-100 in PBS for 15 min at room temperature. After permeabilization, the cells were washed with PBS and blocked with 1% BSA in PBS for 1 hr. The cells were then sequentially stained with the primary antibodies and secondary antibodies, which were diluted in 1% BSA in PBS. DNA was counterstained with DAPI (0.2 μg/ml) in PBS. Details are described in Supplemental Experimental Procedures.

His (Ni-Resin) Pull Down

Transfected cells were solubilized by a brief sonication in denaturing lysis buffer (100 mM sodium dihydrogen phosphate, 10 mM Tris-HCl [pH 8]) containing 6 M guanidine hydrochloride and phosphatase inhibitor cocktail (Sigma-Aldrich), protease inhibitor cocktail (Nakalai Tesque), and phenylmethylsulfonyl fluoride. After centrifugation, the cleared lysates were incubated overnight with cOmplete His-Tag Purification Resin (Roche). The resins were washed once with denaturing wash buffer (100 mM sodium dihydrogen phosphate, 10 mM Tris-HCl, 8M Urea [pH 8.0]), twice with denaturing wash buffer (100 mM sodium dihydrogen phosphate, 10 mM Tris-HCl, 8M Urea [pH 6.3]), and three times with native wash buffer (50 mM sodium dihydrogen phosphate, 300 mM NaCl [pH 8.0]) containing 5 mM imidazole. The bound proteins were eluted with elution buffer (50 mM sodium dihydrogen phosphate, 300 mM NaCl, 250 mM imidazole [pH 8.0]).

SUPPLEMENTAL INFORMATION

Supplemental Information includes seven figures, one table, Supplemental Experimental Procedures, and Supplemental References and can be found with this article online at http://dx.doi.org/10.1016/j.molcel.2014.01.030.

ACKNOWLEDGMENTS

We are grateful to J. Kobayashi, A. Kato, K. Komatsu, Y. Sato, and S. Fukai for reagents and technical support. We thank D. Durocher, A. Shibata, R. Sakasai, and S. Takeda for the critical reading of this manuscript. This work was supported by MEXT KAKENHI Grant (25131708 and 22131006), JSPS KAKENHI Grant (23310040), Health and Labour Sciences Research Grant, the Takeda Science Foundation, and the Uehara Memorial Foundation. A part of this work was carried out under the Cooperative Research Project Program of the Institute of Development, Aging and Cancer at Tohoku University.

Received: July 25, 2013
Revised: October 15, 2013
Accepted: January 23, 2014
Published: February 20, 2014

REFERENCES

Acs, K., Luijsterburg, M.S., Ackermann, L., Salomons, F.A., Hoppe, T., and Dantuma, N.P. (2011). The AAA-ATPase VCP/p97 promotes 53BP1 recruitment by removing L3MBTL1 from DNA double-strand breaks. Nat. Struct. Mol. Biol. *18*, 1345–1350.

Adamson, B., Smogorzewska, A., Sigoillot, F.D., King, R.W., and Elledge, S.J. (2012). A genome-wide homologous recombination screen identifies the RNA-binding protein RBMX as a component of the DNA-damage response. Nat. Cell Biol. *14*, 318–328.

Al-Hakim, A., Escribano-Diaz, C., Landry, M.C., O'Donnell, L., Panier, S., Szilard, R.K., and Durocher, D. (2010). The ubiquitous role of ubiquitin in the DNA damage response. DNA Repair (Amst.) *9*, 1229–1240.

Beucher, A., Birraux, J., Tchouandong, L., Barton, O., Shibata, A., Conrad, S., Goodarzi, A.A., Krempler, A., Jeggo, P.A., and Löbrich, M. (2009). ATM and Artemis promote homologous recombination of radiation-induced DNA double-strand breaks in G2. EMBO J. *28*, 3413–3427.

Bouwman, P., Aly, A., Escandell, J.M., Pieterse, M., Bartkova, J., van der Gulden, H., Hiddingh, S., Thanasoula, M., Kulkarni, A., Yang, Q., et al. (2010). 53BP1 loss rescues BRCA1 deficiency and is associated with triple-negative and BRCA-mutated breast cancers. Nat. Struct. Mol. Biol. *17*, 688–695.

Bunting, S.F., Callén, E., Wong, N., Chen, H.T., Polato, F., Gunn, A., Bothmer, A., Feldhahn, N., Fernandez-Capetillo, O., Cao, L., et al. (2010). 53BP1 inhibits homologous recombination in Brca1-deficient cells by blocking resection of DNA breaks. Cell *141*, 243–254.

Butler, L.R., Densham, R.M., Jia, J., Garvin, A.J., Stone, H.R., Shah, V., Weekes, D., Festy, F., Beesley, J., and Morris, J.R. (2012). The proteasomal de-ubiquitinating enzyme POH1 promotes the double-strand DNA break response. EMBO J. *31*, 3918–3934.

Chapman, J.R., Barral, P., Vannier, J.B., Borel, V., Steger, M., Tomas-Loba, A., Sartori, A.A., Adams, I.R., Batista, F.D., and Boulton, S.J. (2013). RIF1 is essential for 53BP1-dependent nonhomologous end joining and suppression of DNA double-strand break resection. Mol. Cell *49*, 858–871.

Chapman, J.R., Taylor, M.R., and Boulton, S.J. (2012). Playing the end game: DNA double-strand break repair pathway choice. Mol. Cell *47*, 497–510.

Coleman, K.A., and Greenberg, R.A. (2011). The BRCA1-RAP80 complex regulates DNA repair mechanism utilization by restricting end resection. J. Biol. Chem. *286*, 13669–13680.

Di Virgilio, M., Callen, E., Yamane, A., Zhang, W., Jankovic, M., Gitlin, A.D., Feldhahn, N., Resch, W., Oliveira, T.Y., Chait, B.T., et al. (2013). Rif1 prevents resection of DNA breaks and promotes immunoglobulin class switching. Science *339*, 711–715.

Doil, C., Mailand, N., Bekker-Jensen, S., Menard, P., Larsen, D.H., Pepperkok, R., Ellenberg, J., Panier, S., Durocher, D., Bartek, J., et al. (2009). RNF168 binds and amplifies ubiquitin conjugates on damaged chromosomes to allow accumulation of repair proteins. Cell *136*, 435–446.

Escribano-Díaz, C., Orthwein, A., Fradet-Turcotte, A., Xing, M., Young, J.T., Tkáč, J., Cook, M.A., Rosebrock, A.P., Munro, M., Canny, M.D., et al. (2013). A cell cycle-dependent regulatory circuit composed of 53BP1-RIF1 and BRCA1-CtIP controls DNA repair pathway choice. Mol. Cell *49*, 872–883.

Fradet-Turcotte, A., Canny, M.D., Escribano-Díaz, C., Orthwein, A., Leung, C.C., Huang, H., Landry, M.C., Kitevski-LeBlanc, J., Noordermeer, S.M., Sicheri, F., and Durocher, D. (2013). 53BP1 is a reader of the DNA-damage-induced H2A Lys 15 ubiquitin mark. Nature *499*, 50–54.

Goodarzi, A.A., and Jeggo, P.A. (2013). The repair and signaling responses to DNA double-strand breaks. Adv. Genet. *82*, 1–45.

Hu, Y., Scully, R., Sobhian, B., Xie, A., Shestakova, E., and Livingston, D.M. (2011). RAP80-directed tuning of BRCA1 homologous recombination function at ionizing radiation-induced nuclear foci. Genes Dev. *25*, 685–700.

Huen, M.S., Grant, R., Manke, I., Minn, K., Yu, X., Yaffe, M.B., and Chen, J. (2007). RNF8 transduces the DNA-damage signal via histone ubiquitylation and checkpoint protein assembly. Cell *131*, 901–914.

Kim, H., Chen, J., and Yu, X. (2007). Ubiquitin-binding protein RAP80 mediates BRCA1-dependent DNA damage response. Science *316*, 1202–1205.

Kim, J., Daniel, J., Espejo, A., Lake, A., Krishna, M., Xia, L., Zhang, Y., and Bedford, M.T. (2006). Tudor, MBT and chromo domains gauge the degree of lysine methylation. EMBO Rep. *7*, 397–403.

Kolas, N.K., Chapman, J.R., Nakada, S., Ylanko, J., Chahwan, R., Sweeney, F.D., Panier, S., Mendez, M., Wildenhain, J., Thomson, T.M., et al. (2007). Orchestration of the DNA-damage response by the RNF8 ubiquitin ligase. Science *318*, 1637–1640.

Mailand, N., Bekker-Jensen, S., Faustrup, H., Melander, F., Bartek, J., Lukas, C., and Lukas, J. (2007). RNF8 ubiquitylates histones at DNA double-strand breaks and promotes assembly of repair proteins. Cell *131*, 887–900.

Mallette, F.A., Mattiroli, F., Cui, G., Young, L.C., Hendzel, M.J., Mer, G., Sixma, T.K., and Richard, S. (2012). RNF8- and RNF168-dependent degradation of KDM4A/JMJD2A triggers 53BP1 recruitment to DNA damage sites. EMBO J. *31*, 1865–1878.

Mattiroli, F., Vissers, J.H., van Dijk, W.J., Ikpa, P., Citterio, E., Vermeulen, W., Marteijn, J.A., and Sixma, T.K. (2012). RNF168 ubiquitinates K13-15 on H2A/H2AX to drive DNA damage signaling. Cell *150*, 1182–1195.

Nakada, S., Tai, I., Panier, S., Al-Hakim, A., Iemura, S., Juang, Y.C., O'Donnell, L., Kumakubo, A., Munro, M., Sicheri, F., et al. (2010). Non-canonical inhibition of DNA damage-dependent ubiquitination by OTUB1. Nature *466*, 941–946.

Pierce, A.J., Johnson, R.D., Thompson, L.H., and Jasin, M. (1999). XRCC3 promotes homology-directed repair of DNA damage in mammalian cells. Genes Dev. *13*, 2633–2638.

Pommier, Y. (2006). Topoisomerase I inhibitors: camptothecins and beyond. Nat. Rev. Cancer *6*, 789–802.

Saberi, A., Hochegger, H., Szuts, D., Lan, L., Yasui, A., Sale, J.E., Taniguchi, Y., Murakawa, Y., Zeng, W., Yokomori, K., et al. (2007). RAD18 and poly(ADP-ribose) polymerase independently suppress the access of nonhomologous end joining to double-strand breaks and facilitate homologous recombination-mediated repair. Mol. Cell. Biol. *27*, 2562–2571.

Sato, Y., Yamagata, A., Goto-Ito, S., Kubota, K., Miyamoto, R., Nakada, S., and Fukai, S. (2012). Molecular basis of Lys-63-linked polyubiquitination inhibition by the interaction between human deubiquitinating enzyme OTUB1 and ubiquitin-conjugating enzyme UBC13. J. Biol. Chem. *287*, 25860–25868.

Shanbhag, N.M., Rafalska-Metcalf, I.U., Balane-Bolivar, C., Janicki, S.M., and Greenberg, R.A. (2010). ATM-dependent chromatin changes silence transcription in cis to DNA double-strand breaks. Cell *141*, 970–981.

Shao, G., Lilli, D.R., Patterson-Fortin, J., Coleman, K.A., Morrissey, D.E., and Greenberg, R.A. (2009). The Rap80-BRCC36 de-ubiquitinating enzyme complex antagonizes RNF8-Ubc13-dependent ubiquitination events at DNA double strand breaks. Proc. Natl. Acad. Sci. USA *106*, 3166–3171.

Sobhian, B., Shao, G., Lilli, D.R., Culhane, A.C., Moreau, L.A., Xia, B., Livingston, D.M., and Greenberg, R.A. (2007). RAP80 targets BRCA1 to specific ubiquitin structures at DNA damage sites. Science *316*, 1198–1202.

Stewart, G.S., Panier, S., Townsend, K., Al-Hakim, A.K., Kolas, N.K., Miller, E.S., Nakada, S., Ylanko, J., Olivarius, S., Mendez, M., et al. (2009). The RIDDLE syndrome protein mediates a ubiquitin-dependent signaling cascade at sites of DNA damage. Cell *136*, 420–434.

Symington, L.S., and Gautier, J. (2011). Double-strand break end resection and repair pathway choice. Annu. Rev. Genet. *45*, 247–271.

Trojer, P., Li, G., Sims, R.J., 3rd, Vaquero, A., Kalakonda, N., Boccuni, P., Lee, D., Erdjument-Bromage, H., Tempst, P., Nimer, S.D., et al. (2007). L3MBTL1, a histone-methylation-dependent chromatin lock. Cell *129*, 915–928.

Wang, B., Matsuoka, S., Ballif, B.A., Zhang, D., Smogorzewska, A., Gygi, S.P., and Elledge, S.J. (2007). Abraxas and RAP80 form a BRCA1 protein complex required for the DNA damage response. Science *316*, 1194–1198.

Wiener, R., Zhang, X., Wang, T., and Wolberger, C. (2012). The mechanism of OTUB1-mediated inhibition of ubiquitination. Nature *483*, 618–622.

Zhao, G.Y., Sonoda, E., Barber, L.J., Oka, H., Murakawa, Y., Yamada, K., Ikura, T., Wang, X., Kobayashi, M., Yamamoto, K., et al. (2007). A critical role for the ubiquitin-conjugating enzyme Ubc13 in initiating homologous recombination. Mol. Cell *25*, 663–675.

Zimmermann, M., Lottersberger, F., Buonomo, S.B., Sfeir, A., and de Lange, T. (2013). 53BP1 regulates DSB repair using Rif1 to control 5′ end resection. Science *339*, 700–704.

HORM CANC (2013) 4:1–11
DOI 10.1007/s12672-012-0126-6

ORIGINAL PAPER

Intratumoral Estrogen Concentration and Expression of Estrogen-Induced Genes in Male Breast Carcinoma: Comparison with Female Breast Carcinoma

Kiyoshi Takagi · Takuya Moriya · Masafumi Kurosumi · Kimako Oka · Yasuhiro Miki · Akiko Ebata · Takashi Toshima · Shoji Tsunekawa · Hiroyuki Takei · Hisashi Hirakawa · Takanori Ishida · Shin-ichi Hayashi · Junichi Kurebayashi · Hironobu Sasano · Takashi Suzuki

Received: 10 August 2012 / Accepted: 8 October 2012 / Published online: 18 October 2012

Abstract It is speculated that estrogens play important roles in the male breast carcinoma (MBC) as well as the female breast carcinoma (FBC). However, estrogen concentrations or molecular features of estrogen actions have not been reported in MBC, and biological significance of estrogens remains largely unclear in MBC. Therefore, we examined intratumoral estrogen concentrations, estrogen receptor (ER) α/ERβ status, and expression profiles of estrogen-induced genes in MBC tissues, and compared these with FBC. 17β-Estradiol concentration in MBC (n=4) was significantly (14-fold) higher than that in non-neoplastic male breast (n=3) and tended to be higher than that in FBC (n=7). Results of microarray analysis clearly demonstrated that expression profiles of the two gene lists, which were previously reported as estrogen-induced genes in MCF-7 breast carcinoma cell line, were markedly different between MBC and FBC. In the immunohistochemistry, MBC tissues were frequently positive for aromatase (63 %) and 17β-hydroxysteroid dehydrogenase type 1 (67 %), but not for steroid sulfatase (6.7 %). A great majority (77 %) of MBC showed positive for both ERα and ERβ, and its frequency was significantly higher than FBC cases. These results suggest that estradiol is locally produced in MBC

K. Takagi (✉) · T. Suzuki
Department of Pathology and Histotechnology,
Tohoku University Graduate School of Medicine,
2-1 Seiryo-machi, Aoba-ku,
Sendai, Miyagi-ken 980-8575, Japan
e-mail: k-takagi@med.tohoku.ac.jp

T. Moriya
Department of Pathology 2, Kawasaki Medical School,
Kurashiki, Japan

M. Kurosumi
Department of Pathology, Saitama Cancer Center,
Saitama, Japan

K. Oka · H. Hirakawa
Department of Surgery, Tohoku Kosai Hospital,
Sendai, Japan

Y. Miki · H. Sasano
Department of Anatomic Pathology,
Tohoku University Graduate School of Medicine,
Sendai, Japan

A. Ebata · T. Ishida
Department of Surgical Oncology,
Tohoku University Graduate School of Medicine,
Sendai, Japan

T. Toshima
Department of Surgery, Tohoku Rosai Hospital,
Sendai, Japan

S. Tsunekawa
Department of Surgery, Kansai Electric Power Hospital,
Osaka, Japan

H. Takei
Division of Breast Surgery, Saitama Cancer Center,
Saitama, Japan

S.-i. Hayashi
Department of Molecular and Functional Dynamics,
Tohoku University Graduate School of Medicine,
Sendai, Japan

J. Kurebayashi
Department of Breast and Thyroid Surgery,
Kawasaki Medical School,
Kurashiki, Japan

H. Sasano
Department of Pathology, Tohoku University Hospital,
Sendai, Japan

tissue by aromatase. Different expression profiles of the estrogen-induced genes may associate with different estrogen functions in MBC from FBC, which may be partly due to their ERα/ERβ status.

Introduction

Male breast carcinoma (MBC) is an uncommon disease, and its incidence is less than 1 % of that in female breast carcinoma (FBC). However, it has been increasing in recent years [1]. Because of the low incidence, MBC has not been studied well, and limited information is available regarding the epidemiology, pathogenesis, and treatment [2]. Therefore, it is very important to examine the biological features of MBC in order to improve clinical outcome of the patients.

It is well known that estrogens contribute immensely to the development and/or progression of FBC. Concentration of biologically active estrogen estradiol is significantly high in FBC tissues, and it is locally produced from circulating inactive steroids by estrogen-producing enzymes, such as aromatase (conversion from circulating androstenedione to estrone or testosterone to estradiol), steroid sulfatase (STS; hydrolysis of circulating estrone sulfate to estrone), and 17β-hydroxysteroid dehydrogenase type 1 (17βHSD1; conversion of estrone to estradiol) [3]. Estrogen actions are initiated by binding of estrogens with estrogen receptors (i.e., ERα or ERβ), followed by transactivation of the target genes. Various estrogen-responsive genes have been identified in the breast carcinoma [4, 5], and analyses of these genes have greatly contributed to better understanding of molecular functions of estrogen actions in FBC [6]. The estrogen actions are considered to be mainly mediated through ERα in FBC [7, 8], and endocrine therapies, such as anti-estrogens (tamoxifen, etc.), aromatase inhibitors, and gonadotropin-releasing hormone (GnRH) agonists, are used in patients with ERα-positive FBC patients.

Estrogens are also speculated to play important roles in MBC, and tamoxifen is used in MBC patients as an endocrine therapy [9]. Various studies have demonstrated frequent expression of ERα in MBC tissues as well as ERβ and progesterone receptor (PR) [10–12], and immunolocalization of aromatase has been also reported in MBC [13]. However, intratumoral concentration of estrogens or expression of other estrogen-producing enzymes has not been reported in MBC. Moreover, no information is available regarding the expression profiles of estrogen-responsive genes in MBC, to the best of our knowledge. Therefore, it remains unclear whether estrogen actions and/or effectiveness of endocrine therapy in MBC could be the same as that in FBC.

Therefore, in this study, we examined intratumoral concentrations of estrogens, immunolocalization of estrogen-producing enzymes, and expression profiles of estrogen-induced genes in MBC tissues, and compared these findings with those in FBC, in order to examine the significance of estrogens in MBC.

Materials and Methods

Patients and Tissues

Two sets of tissue specimens were used in this study. The first set is composed of 14 snap-frozen specimens. Among these, four MBC tissues were obtained from patients who underwent surgical treatment from 2009 to 2010 at Tohoku University Hospital (Sendai, Japan), Tohoku Kosai Hospital (Sendai, Japan), Tohoku Rosai Hospital (Sendai, Japan), and Kansai Electric Power Hospital (Osaka, Japan). The mean age of these patients was 65 years (range, 62–67). Three non-neoplastic breast tissues were also collected from patients who underwent surgical treatment at Tohoku University Hospital, Tohoku Kosai Hospital, and Saitama Cancer center (Saitama, Japan; mean age, 65 years; range, 62–67 years), which were not matched with the carcinoma specimens. As a control group, seven specimens of FBC were obtained from postmenopausal patients who underwent surgical treatment from 2001 to 2003 at Tohoku University Hospital (mean age, 57 years; range, 50–69 years). These specimens were stored at −80 °C for subsequent hormone assays. Eight specimens of MBC and FBC were also used in microarray analysis.

The second set is composed of 102 specimens of breast carcinomas fixed in 10 % formalin and embedded in paraffin wax. Among these, 30 MBC tissues were obtained from patients who underwent surgical treatment from 1975 to 2010 at Tohoku University Hospital, Tohoku Kosai Hospital, Tohoku Rosai Hospital, Saitama Cancer Center, Sendai, and Kawasaki Medical School Hospital (Okayama, Japan). As a control group, we also used 72 FBC tissues collected from postmenopausal women who underwent surgical treatment from 1984 to 1992 at Tohoku University Hospital.

Research protocol was approved by Ethics Committee at Tohoku University School of Medicine.

Liquid Chromatography/Electrospray Tandem Mass Spectrometry (LC-MS/MS)

Concentrations of estradiol, estrone, testosterone, and androstenedione were measured by LC-MS/MS analysis in ASKA Pharma Medical Co., Ltd. (Kawasaki, Japan), as described previously [14, 15]. In the evaluation of estradiol concentration, we measured only 17β-estradiol, but not 17α-estradiol in this study. Briefly, tissue specimens were homogenized in 1 mL of distilled water, and steroid fraction was extracted with diethyl ether. In this study, we used an LC (Agilent 1100, Agilent Technologies, Waldbronn, Germany) coupled with an API 4000 triple-stage quadrupole